



Response of chromophoric dissolved organic matter dynamics to tidal oscillations and anthropogenic disturbances in a large subtropical estuary

Yongqiang Zhou^{a,b}, Yuan Li^{a,c}, Xiaolong Yao^{a,b}, Wenhao Ding^{a,b}, Yibo Zhang^{a,b}, Erik Jeppesen^{d,e}, Yunlin Zhang^{a,b,*}, David C. Podgorski^f, Chunmei Chen^g, Yi Ding^h, Huawu Wu^a, Robert G.M. Spencerⁱ

^a Taihu Laboratory for Lake Ecosystem Research, State Key Laboratory of Lake Science and Environment, Nanjing Institute of Geography and Limnology, Chinese Academy of Sciences, Nanjing 210008, China

^b University of Chinese Academy of Sciences, Beijing 100049, China

^c School of Tourism and City Management, Zhejiang Gongshang University, Hangzhou 310018, China

^d Department of Bioscience and Arctic Research Centre, Aarhus University, Vejløvej 25, DK-8600 Silkeborg, Denmark

^e Sino-Danish Centre for Education and Research, Beijing 100190, China

^f Pontchartrain Institute for Environmental Sciences, Department of Chemistry, University of New Orleans, New Orleans 70148, LA, USA

^g Zhejiang University of Water Resources and Electric Power, Hangzhou 310018, China

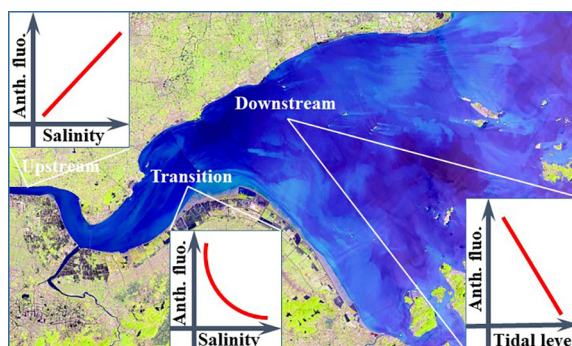
^h Zhejiang Hydrology Bureau, Hangzhou 310009, China

ⁱ Department of Earth, Ocean and Atmospheric Science, Florida State University, Tallahassee 32306, FL, USA

HIGHLIGHTS

- Qiantang estuary is subjected to strong tides and anthropogenic disturbances.
- Tide influences physical mixing of riverine freshwater and saltwater.
- Anthropogenic input contributed primarily to the CDOM pool in the estuary.
- Decreased tidal levels are often linked to enhanced anthropogenic CDOM.

GRAPHICAL ABSTRACT



ARTICLE INFO

Article history:

Received 30 October 2018

Received in revised form 28 December 2018

Accepted 20 January 2019

Available online 24 January 2019

Editor: Yolanda Picó

Keywords:

Chromophoric dissolved organic matter (CDOM)

Parallel factor analysis (PARAFAC)

ABSTRACT

Estuaries support the livelihood of ~75% of the world's population and maintain high primary production in coastal waters, which are often subjected to strong tides and anthropogenic disturbances. There is a paucity of information on how the optical composition and bioavailability of chromophoric dissolved organic matter (CDOM) are influenced by tidal oscillations in estuaries with highly urbanized surrounding areas. We examined the semi-diurnal Qiantang Bore, one of the Earth's three most predominant tide bores, and found that dissolved organic carbon (DOC), CDOM absorption $a(254)$ and terrestrial humic-like C1, tryptophan-like C2 and C5, fulvic-like C3, and microbial humic-like C4 decreased markedly with increasing salinity. This suggests that physical mixing of riverine freshwater and saltwater can shape the optical composition of CDOM in the estuary. This was supported by the semi-diurnally and hourly observations at Zhijiang (salinity ~0.1‰, upstream of the estuary) that DOC, bioavailable DOC (BDOC), C1–C2, and C4–C5 increased markedly with decreasing tidal level, while DOC and C1–C5 increased notably with increasing salinity. We further found $\delta^{18}\text{O}$ was enriched with increasing

* Corresponding author at: Nanjing Institute of Geography and Limnology, Chinese Academy of Sciences, 73 East Beijing Road, Nanjing 210008, China.
E-mail address: ylzhang@niglas.ac.cn (Y. Zhang).

Tidal oscillations
Qiantang estuary
Ultrahigh resolution mass spectrometry

tidal level, while tryptophan-like C2 and C5, and fulvic-like C3 decreased significantly with increasing tidal level at Zhapu (salinity ~7‰, downstream of the estuary). Furthermore, DOC, BDOC, C1, and C4 decreased, while $\delta^{18}\text{O}$ and C3 increased markedly with increasing salinity. Further evidences come from the notably lower mean first principal component (PC1) scores at Zhijiang and Zhapu, both positively associated with anthropogenic tryptophan-like inputs, were observed during ebb than during flood tides, and PC1 at Zhijiang increased notably with increasing salinity. We conclude that anthropogenic inputs contributed primarily to the CDOM pool in the estuary and are mediated by the physical mixing of riverine freshwater and seawater, and ebb tides are often associated with enhanced anthropogenic CDOM with relatively high bioavailability.

© 2019 Elsevier B.V. All rights reserved.

1. Introduction

Estuaries and coastal ecosystems support the livelihood of ~75% of the world's population (Paerl et al., 2013), and anthropogenic impacts (e.g. industrialization, urbanization, and agricultural production) in these areas have resulted in increasing concentrations of terrestrial and anthropogenic dissolved organic matter (DOM) in receiving coastal environments (Paerl and Huisman, 2008; Huang et al., 2018). Correspondingly, ~30% of primary production in the global oceans occurs in these coastal waters (Yamashita et al., 2008). The intense primary productivity leads to the production and high concentration of autochthonous DOM in these waters. Thus, the fate of terrestrial, anthropogenic, and autochthonous DOM in these ecosystems can be complex. Stresses imposed by climatic, anthropogenic, and tidal perturbations have accelerated the production and degradation processes of DOM in coastal waters (Stedmon and Markager, 2005a; Yamashita et al., 2008; Osburn et al., 2012; Guo et al., 2014). Flood- and tidal-induced water mixing and the biological and photochemical degradation of DOM in coastal waters can also fuel the outgassing of greenhouse gases and in this way impact the global climate change (Bianchi et al., 2013). Therefore, numerous studies have been completed to elucidate how upstream tributary water inputs may impact the optical dynamics of DOM in receiving coastal waters (Stedmon and Markager, 2005a; Yang et al., 2013; Guo et al., 2014). Ebb and flood tides control the mixing of riverine freshwater and backward-propagated saltwater and greatly change the inundation areas of estuaries and coastal environments (Carey and Fulweiler, 2014) and may thus influence the biogeochemical processing of DOM. Previous studies have shown that tidal oscillations impact the water level, discharge, concentration of suspended particulate matter (SPM), and residence time of silica (Carey and Fulweiler, 2014; Shen et al., 2016). However, little is known about how tidal oscillations in highly urbanized estuary areas may affect the compositional dynamics of DOM.

Tropical cyclone activity has intensified in all the oceans worldwide and this, as well as increased intensity of land-falling typhoons over the Pacific Ocean since the late 1970s (Mei and Xie, 2016), can change the

mixing behavior of water masses and the optical dynamics of DOM (Osburn et al., 2012; Zhou et al., 2016c). The ongoing climate change-induced intensification of tropical cyclones coupled with astronomical tides will potentially result in enhanced tidal oscillations in estuaries and coastal waters. Flood tides superimposed with storm surges can blow seawater backwards far inland along floodplains, this being extremely pronounced in the three most predominant tidal bores worldwide: the Qiantang estuary, China (Xie et al., 2017), the Ganges estuary, Bangladesh (Nicholls et al., 2016), and the Amazon estuary, Brazil (Ward et al., 2015).

The Qiantang tidal bore is created by a combination of gravity in the Earth's rotation, the backwater effect induced by the tide and the Qiantang River flow, and the horn-shaped entrance of the estuary itself (Fig. 1). The Qiantang bore can be categorized as a semi-diurnal tide, and the difference in tidal levels of ebb and flood tides at regions downstream of Zhijiang and upstream of Zhapu can be as high as 6 m (Fig. S1; Fig. S2), this being especially pronounced under typhoon conditions. Ebb and flood tides in the estuary create a big tidal-flat area, especially in the northern half of the estuary, where tremendous exchange of freshwater and saltwater currents, together with physical mixing of surface and deep layers of the water columns coexist. The tidal oscillations of the Qiantang bore in the highly urbanized estuary area may therefore have a great impact on the optical compositional dynamics of CDOM. To date, however, the direct relationship between tidal oscillations and the optical property and bioavailability of DOM in tide-dominated estuaries remains to be elucidated.

The objective of this study was to unravel how tidal oscillations impact the optical compositional dynamics of DOM and its bioavailability in the Qiantang estuary with surrounding highly urbanized residential areas. A study combining measurements of extensive sampling, semi-diurnal and hourly CDOM EEMs fluorescence, $\delta^{18}\text{O}$, $\delta^{13}\text{C}$ -DOC, bioavailable DOC (BDOC), and FT-ICR MS for the samples collected from upstream Zhijiang to downstream Zhapu and the regions between these two sites was carried out to investigate how CDOM optical compositional dynamics may be impacted by tidal oscillations in the highly urbanized estuary. We hypothesized that the tidal oscillations of the

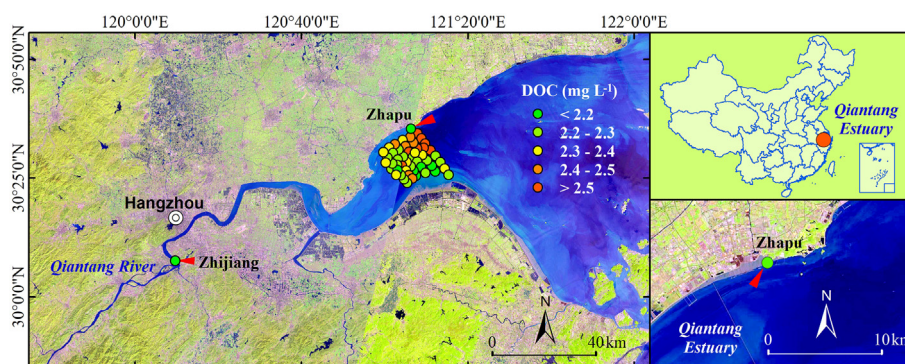


Fig. 1. Location of sampling sites and the corresponding concentrations of dissolved organic carbon (DOC). Red triangles show the location of tidal gauging stations. Magenta-colored region surrounding the Zhijiang sampling site is the metropolitan city of Hangzhou.

highly urbanized Qiantang estuary impact the physical mixing of riverine freshwater inputs and seawater in the estuary and, thereby, both the optical composition and the bioavailability of CDOM molecules.

2. Materials and methods

2.1. Study sites and sample collection

The Qiantang estuary is located south of the Lake Taihu Basin and is one of the most developed areas in China. The Qiantang bore is one of the world's three largest tidal bores. It has a horn-shaped entrance with a width of ~95 km after which it gradually narrows to a width of ~3 km at the inlet of the estuary. This, coupled with the backwater effect induced by the tide and the Qiantang River, the largest river in the Zhejiang Province in China, leads to the formation of huge waves semi-diurnally in the regions from downstream of Zhapu back to upstream of Zhijiang (Fig. 1).

A total of 437 grab surface (0.5 m) water samples were collected from the Qiantang estuary, including an extensive field sampling campaign (50 sites, Fig. 1) conducted in the estuary during daytime from 8:00 a.m. to 16:00 p.m. from 25 July to 27 July 2017 and continuous semi-diurnal from 31 October 2016 to 19 November 2016 or hourly (from around 8:00 a.m. to 16:00 p.m. on 6, 12, 16, and 18 November 2016) observations at Zhijiang (66 × triplicate samples, salinity ~0.1‰, upstream) and Zhapu (63 × triplicate samples, salinity ~7‰, downstream) (Fig. S1; Fig. S2). Due to the large difference in tidal levels and semi-diurnally transformation between ebb and flood tides, samples were collected semi-diurnally for less than a month being able to capture an astronomical tide and hourly for four daytime (Table S1; Fig. S3), and the extensive campaign was conducted one time. The sampling time was able to cover a uniform distribution of tidal levels at both Zhijiang (upstream) and Zhapu (downstream) (Table S1; Fig. S3). Salinity and fluorescent DOM (FDOM) concentrations (in quinine sulfate unit, QSU) at depth of 0.5 m were measured in situ using a YSI EXO2 multi-parameter water quality sonde (Yellow Springs Inc., OH, USA). Surface (0–0.5 m) water samples were collected in 2.5 L acid-cleaned Niskin bottles and stored on ice while in the field. Samples were immediately transported to the laboratory where they were filtered upon arrival and then stored in the dark at 4 °C. CDOM optical measurements were undertaken within two days and all laboratory measurements were finished within five days. Filtered samples were frozen for other analyses.

2.2. Hydrological data

Data on the hourly flow rate and tidal level at Zhijiang from 0:00 a.m. on 31 October 2016 to 0:00 a.m. on 20 November 2016 were provided by the Zhijiang Hydrologic Station and were well-validated by the Taihu Basin hydrological information service system (<http://218.1.102.99:8100/indexWater.html>). Information on the hourly tidal level at Zhapu from 0:00 a.m. on 31 October 2016 to 0:00 a.m. on 20 November 2016 were freely available from the Chinese Naval service system (<http://www.cnss.com.cn/>).

2.3. DOC, bioavailable DOC (BDOC), CDOM absorption, fluorescence measurements, and PARAFAC modeling

Excitation-emission matrix spectroscopy (EEMs) provides a marked increase in the optical resolution over absorption spectra as it enables the differentiation of CDOM that absorbs light at the same wavelength while emitting it in distinct spectral regions (Murphy et al., 2008). EEMs coupled with parallel factor analysis (PARAFAC) have been shown to have considerable advantage over the traditional “peak picking” technique in resolving the fluorescent compositional dynamics of CDOM (Murphy et al., 2008; Stedmon and Bro, 2008; Murphy et al., 2013; Yang et al., 2017).

Detailed information about CDOM absorption and fluorescence measurements, the calibration procedures for EEMs spectra, and PARAFAC modeling can be found in the Supporting Information. Split-half validation analysis, random initialization analysis, the analysis of residuals (Stedmon and Bro, 2008; Murphy et al., 2013) all validated a six-component model (Fig. S4; Fig. S5; Fig. S6).

Water samples were filtered through Whatman GF/F (0.7 μm) filters and evaluated for DOC measurements using a TOC-V CPN (Shimadzu, Tokyo, Japan) analyzer with NPOC mode by combustion at ~680 °C. All field samples collected from Zhijiang and Zhapu were measured for DOC biodegradability. In this study, BDOC is defined as percent DOC mineralized over 28 days as recommended by Vonk et al. (2015). After initial collection and filtration of the samples in the field, 50 mL aliquots from each field sample were filtered through pre-rinsed 0.22 μm Millipore membrane cellulose filters to remove bacteria and then placed in 70 mL brown glass incubation vials. Site-specific raw water was used as bacterial inoculum and 2 mL of this site-specific bacterial inoculum was added to each incubation vial. All vials were kept oxygenated at room temperature (20 ± 2 °C) and received a nutrient amendment, and the ambient concentrations were increased by 80 μM NH₄⁺-N and 10 μM PO₄³⁻-P to relieve nutrient limitation of DOC processing as recommended by Holmes et al. (2008) and Abbott et al. (2014). The vials were shaken gently several times every day and the incubated samples were re-filtered through Millipore filters after 28 days' incubation to determine the DOC concentration again.

2.4. Stable isotopes (δ¹⁸O, δ¹³C-DOC) and SPM measurements

Water stable isotope δ¹⁸O can be used to trace the source of water mass as evaporation can result in enriched δ¹⁸O values (Yamamoto-Kawai et al., 2008). δ¹⁸O samples were collected from 0.2 m depth and measured on an LGR DLT-100 (model:908-0008) Laser Adsorption Spectroscopy (Los Gatos Research, Inc. Mountain View, CA, USA), and δ¹⁸O was calibrated against Vienna Standard Mean Ocean Water with precision ≤0.3‰ (Wu et al., 2015).

δ¹³C-DOC can be used to examine the source of bulk-DOC as δ¹³C-DOC of terrestrial DOC and autochthonous DOC typically range between -29‰ and -26‰ (similar to that of C3 plants) and between -25‰ and -20‰ (similar to that of C4 plants), respectively (Hood et al., 2009; Zhou et al., 2017). The samples from Zhijiang and Zhapu were all filtered through Whatman GF/F filters to measure bulk δ¹³C-DOC. All samples were dried at 55 ± 5 °C in acid-cleaned beakers to constant weight (generally within three days). The CDOM residue was exposed to 5 mol L⁻¹ HCl solutions for ~24 h to steam acidify CDOM samples to remove dissolved inorganic carbon. The solid residue was dried again at 55 ± 5 °C for 24 h and then combusted with a Flash EA1112 analyzer. The CO₂ gas produced was subsequently measured on a Thermo Finnigan MAT Deltaplus dual-inlet continuous flow isotope ratio mass spectrometer with a precision of <0.1‰. Bulk δ¹³C-DOC was calibrated against the Vienna Pee Dee Belemnite (VPDB) standard (Hood et al., 2009; Zhou et al., 2017).

Whatman GF/F filters were combusted at 550 °C for 4 h and weighed using an electrobalance with an accuracy of <10⁻² mg. Water samples (>100 mL according to the amount of particles) were first filtered through GF/F filters, which were subsequently dried at 105 °C for 4 h and weighed again to calculate SPM concentrations (Zhou et al., 2016b).

2.5. Fourier transform ion cyclotron resonance mass spectrometry (FT-ICR MS) and data analyses

Samples collected from Zhijiang and Zhapu (one sample from each site) on 6 November 2016 were solid-phase extracted using PPL Bond Elut (Agilent) resins prior to analysis by negative-ion electrospray FT-ICR MS (Spencer et al., 2014). Briefly, ~40 mL samples (filtered through 0.22 μm Millipore filters and volumes calculated based on the DOC concentrations to allow extraction of a similar load of DOC with each

cartridge) were thawed and acidified to pH = 2 with 10 M HCl (32%, reagent grade, p.a. quality). The acidified samples were slowly passed through the PPL cartridges (~5 mL min⁻¹). Two 3 mL of 0.01 M HCl were then passed through the cartridges to wash away any inorganic carbon before the cartridges were dried under pure nitrogen gas. DOM was finally eluted from the cartridges using 1 mL of methanol and stored at -20 °C in the dark. A Milli-Q water sample was also solid-phase extracted, eluted, and used as procedural blank during the FT-ICR MS analyses. The methanol extracts from the PPL cartridges were subsequently diluted 1:1 using Milli-Q water and determined with a 21 T FT-ICR MS (Bruker, USA) at the National High Magnetic Field Laboratory, Tallahassee, Florida, USA (Smith et al., 2018). Molecular formulas were assigned to signals >6σ RMS baseline noise with EnviroOrg ©,™ (Corilo, 2015). The mass measurement accuracy of the assigned formulas did not exceed <0.3 ppm after internal calibration. van Krevelen diagrams displaying elemental ratios of H/C vs. O/C can be used to examine the potential sources and compositional dynamics of DOM (Stubbins et al., 2010; Ohno et al., 2014; Spencer et al., 2014). The classification of molecular formulas was performed following the methods detailed in Ohno et al. (2014). Briefly, the biomolecular chemical classes categorized via the van Krevelen diagrams in this study typically include: (a) lipids (O/C = 0–0.3, H/C = 1.5–2.0), (b) proteins and amino acids (O/C = 0.3–0.67, H/C = 1.5–2.2), (c) lignins (O/C = 0.1–0.67, H/C = 0.7–1.5), (d) carbohydrates (O/C = 0.67–1.2, H/C = 1.5–2.2), (e) unsaturated hydrocarbons (O/C = 0–0.1, H/C = 0.7–1.5), (f) condensed aromatics (O/C = 0–0.67, H/C = 0.2–0.7), and (g) tannins (O/C = 0.67–1.2, H/C = 0.5–1.5) (Ohno et al., 2014).

2.6. Principal component analysis (PCA) modeling

Principal components analysis (PCA) was performed to produce a reduced data set summarizing the majority of variables without prior knowledge of the data array itself (Bro and Smilde, 2014). Due to the distinct characteristics of CDOM quality between Zhijiang and Zhapu, we conducted PCA for the two sites separately. Physico-chemical variables, including SPM, δ¹³C-DOC, DOC, BDOC, as well as the six PARAFAC components C1–C6, were all included in the PCA based on the Pearson correlation matrices among these variables and the corresponding significance levels (Fig. S7). The complete data array was first auto-scaled before PCA modeling (Bro and Smilde, 2014). Scree test is the eigenvalues plotted as a function of the number of components with the assumption that relevant information is larger than random noise (Bro and Smilde, 2014). The scree result of PCA eigenvalues indicated that the first two components explained the majority of the variability included in the PCA models for both Zhijiang and Zhapu (Fig. S8).

2.7. Statistical analyses

The location of sampling sites and tidal gauging stations was mapped with ArcGIS 10.2 software. EEMs contour plot and linear and nonlinear fittings were established using MATLAB R2015b. PCA in this study was performed using the inbuilt statistics toolbox in MATLAB. Means and standard deviations (S.D.) were determined and *t*-tests performed using R i386 2.15.2. Results of *t*-test and linear and nonlinear fittings with *p* < 0.05 were recorded as significant.

3. Results

3.1. PARAFAC components

The six-component model explained over 99.9% of the total variability of the EEMs data array (Fig. S4) and was validated using the split-half validation and random initialization procedure (Fig. S5; Fig. S6). The spectral shapes of the six PARAFAC components were compared with those identified earlier in other aquatic ecosystems using an online

CDOM fluorescence library – Openfluo (Murphy et al., 2014). C1 exhibited two Ex maxima (at 240 and 345 nm) and a single Em maximum (at 468 nm) (Fig. S4) and can be characterized as a terrestrial humic-like fluorophore (Kowalczyk et al., 2009; Murphy et al., 2011; Kothawala et al., 2014; Shutova et al., 2014). C2 (230 (280)/340 nm) and C5 (275/324 nm) can be categorized as an amino-acid-like associated tryptophan-like fluorophore (Fig. S4) (Stedmon and Markager, 2005a; Murphy et al., 2011). The two components can be originated from the presence of polyphenolic moieties in DOM (Maie et al., 2007; Hur et al., 2011), or biodegradation of algae cells (Zhou et al., 2015) and anthropogenic sewages (Stedmon et al., 2011; Zhou et al., 2016a). C3 displayed one Ex maximum (at 230 nm) and one Em maximum (at 428 nm) (Fig. S4) and was categorized as an agricultural humic-like fluorophore (Kowalczyk et al., 2009; Osburn et al., 2011; Osburn et al., 2012; Shutova et al., 2014). C4 exhibited two Ex maxima (at 240 and 305 nm) and one Em maximum (at 380 nm) (Fig. S4) and was characterized as a typical microbial humic-like fluorophore (Murphy et al., 2011; Osburn et al., 2011). C6 had spectral shapes (230 (270)/300 nm) similar to those of tyrosine-like fluorophores (Fig. S4) (Murphy et al., 2011; Kowalczyk et al., 2013).

3.2. Spatial variability of CDOM optical properties in the estuary

For the samples collected in the extensive field campaign in July 2017, salinity ranged from 4.9 to 8.4‰ with a mean of 6.0 ± 0.8‰ and increased notably from the upstream to the downstream of the estuary (Fig. 2), and this was especially pronounced in the southern half of the channel (Fig. 2). This reflects a physical mixing of riverine freshwater and saltwater. DOC concentrations decreased gradually from 2.9 mg L⁻¹ in the areas near Zhapu (salinity ~7‰, downstream) to 2.2 mg L⁻¹ at the south shallow shore of the estuary (Fig. 1). In comparison, the maximum fluorescence intensity (*F*_{max}) of terrestrial humic-like C1, tryptophan-like C2, and agricultural humic-like C3 decreased gradually from the upstream to the downstream (seaward) reach of the estuary, and the trends were especially pronounced in the southern half of the estuary (Fig. 2). We found that DOC, CDOM absorption *a* (254), in situ measured FDOM concentrations, and the *F*_{max} of all the six components except for C6 decreased notably with increasing salinity (*p* < 0.01, Fig. 2). If we only take into account the data from the southern half of the channel, the area that best represent the physical mixing of freshwater and seawater, the determination coefficients of linear and nonlinear fittings between salinity and CDOM-related indices increased but the relationship patterns remained similar (Fig. S9).

3.3. Daily and hourly variations of tidal oscillations and CDOM optical composition

The Qiantang bore exhibited semi-diurnal fluctuations. Thus, the flood tides occurred at 3:00–6:00 a.m. and 16:00–19:00 p.m. for Zhijiang and at 0:00–3:00 a.m. and 13:00–16:00 p.m. for Zhapu during the sampling period (Fig. S1; Fig. S2; Table S1). During the sampling period, no significant difference appeared between the mean tidal level at Zhijiang (3.9 ± 0.7 m) and Zhapu (4.06 ± 1.99 m) (Table 1; Fig. S1; Fig. S2). We found significantly higher mean SPM and BDOC at Zhapu than at Zhijiang (*t*-test, *p* < 0.001; Table 1; Fig. S1; Fig. S2), while no significant difference was observed between the mean DOC concentrations at Zhijiang and Zhapu (*t*-test, *p* > 0.05; Table 1; Fig. S1; Fig. S2). We further discovered a significantly depleted mean bulk δ¹³C-DOC at Zhijiang than at Zhapu (*t*-test, *p* < 0.001; Table 1; Fig. S1; Fig. S2). The two amino-acid-like associated tryptophan-like fluorophores, C2 and C5, contributed predominantly to the CDOM fluorescence, and their summed contribution percentages to the fluorescence intensity (*F*_{max}) of the six components ranged from 64.2% to 90.6% with a mean of 79.5% ± 6.2% (Table 1; Fig. S1; Fig. S2). Specifically, the mean *F*_{max} levels of terrestrial humic-like C1 and agricultural humic-like C3, tryptophan-like C2 and C5, and microbial humic-like C4 at Zhijiang were all remarkably lower

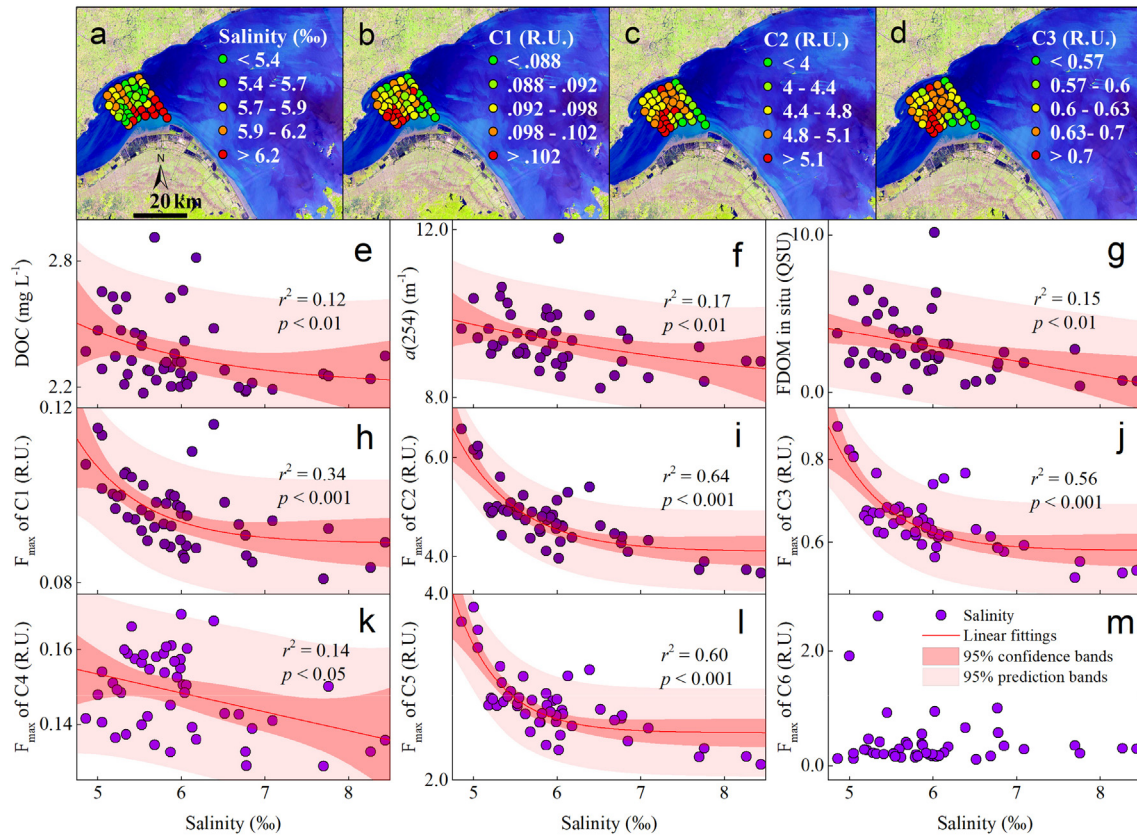


Fig. 2. Spatial variations of salinity (a) and PARAFAC-derived C1–C3 (b–d) for the samples collected from the Qiantang estuary. Relationships between salinity and dissolved organic carbon (DOC) (e), CDOM absorption $a(254)$ (f), and in situ measured FDOM concentration (g), and the fluorescence intensity of the six PARAFAC components C1–C6 (h–m) for the samples collected from the estuary. Dark and light pink shaded areas in panels e–l are 95% confidence and prediction bands, respectively.

than at Zhapu (t -test, $p < 0.001$; Table 1; Fig. S1; Fig. S2). In comparison, the mean F_{max} of tyrosine-like C6 was significantly higher at Zhijiang than that at Zhapu (t -test, $p = 0.018$; Table 1; Fig. S1; Fig. S2).

3.4. Relationships between tidal oscillations and CDOM optical composition

At Zhijiang, significant negative relationships were recorded between tidal level and DOC, BDOC, F_{max} values of terrestrial humic-like C1, tryptophan-like C2 and C5, and microbial humic-like C4 ($p < 0.01$, Fig. 3). No significant relationship was observed between tidal level and $\delta^{18}O$, $\delta^{13}C$ -DOC, agricultural humic-like C3 or tyrosine-like C6 (Fig. 3). There were two clusters in the relationships between tidal levels and CDOM-related indices and the clusters showed different trends against tidal level (Fig. S10). If we exclude the small cluster of data from linear fittings, weak positive relationships were found between tidal level and $\delta^{18}O$, tryptophan-like C2 and C5, and a significant

negative relationship was detected between tidal level and agricultural humic-like C3 (Fig. S10). In comparison, significant positive relationships were found between salinity and DOC, C1–C5 (Fig. S11), while no significant relationship was traced between salinity and $\delta^{18}O$, $\delta^{13}C$ -DOC or C6 (Fig. S11). There were two clusters in the relationships between salinity and C3 and both clusters showed different trends against salinity (Fig. S11) and if we remove the small cluster of data from fitting, a close and positive relationship emerged (Fig. S11). Note that laboratory salt addition (KCl, reagent grade) does not change fluorescent spectra of CDOM samples (Fig. S12).

At Zhapu, significant positive relationships were observed between tidal level and $\delta^{18}O$ ($p < 0.05$, Fig. 4), while significant negative relationships were recorded between tidal level and tryptophan-like C2 and C5, as well as agricultural humic-like C3 ($p < 0.01$, Fig. 4). No significant relationship was traced between tidal level and DOC, BDOC, or the F_{max} values of C1, C4, and C6 (Fig. 4). In comparison, significant negative

Table 1

Summary of hydrological, physico-chemical, and DOM compositional parameters (mean \pm S.D.) for the samples collected from Zhijiang and Zhapu and the significance level of differences between the two sites using t -test.

Sampling sites	Tidal level (m)	Flow rate (m ³ s ⁻¹)	Salinity (‰)	$\delta^{18}O$ (‰)	SPM (mg L ⁻¹)	DOC (mg L ⁻¹)	BDOC (%)
Zhijiang	3.94 \pm 0.68	838 \pm 2392	0.10 \pm 0.01	-6.5 \pm 0.3	60.8 \pm 60.2	2.06 \pm 0.16	11.1 \pm 6.3
Zhapu	4.06 \pm 1.99	n.a.	6.91 \pm 0.39	-4.9 \pm 0.3	862.6 \pm 553.1	2.17 \pm 1.00	20.6 \pm 16.8
p	>0.05	n.a.	<0.001	<0.001	<0.001	>0.05	<0.001
Sampling sites	$\delta^{13}C$ -DOC (%)	C1 (R.U.)	C2 (R.U.)	C3 (R.U.)	C4 (R.U.)	C5 (R.U.)	C6 (R.U.)
Zhijiang	-26.0 \pm 0.2	0.15 \pm 0.01	2.09 \pm 0.82	0.15 \pm 0.07	0.25 \pm 0.02	1.88 \pm 0.68	0.39 \pm 0.21
Zhapu	-25.8 \pm 0.3	0.22 \pm 0.02	4.71 \pm 0.51	0.31 \pm 0.07	0.28 \pm 0.03	4.10 \pm 0.41	0.31 \pm 0.11
p	<0.01	<0.001	<0.001	<0.001	<0.001	<0.001	0.018

SPM: suspended particulate matter; DOC: dissolved organic carbon; BDOC: bioavailable DOC; $\delta^{13}C$ -DOC: stable isotope $\delta^{13}C$ -DOC; C1–C6: the six PARAFAC-derived fluorescent components.

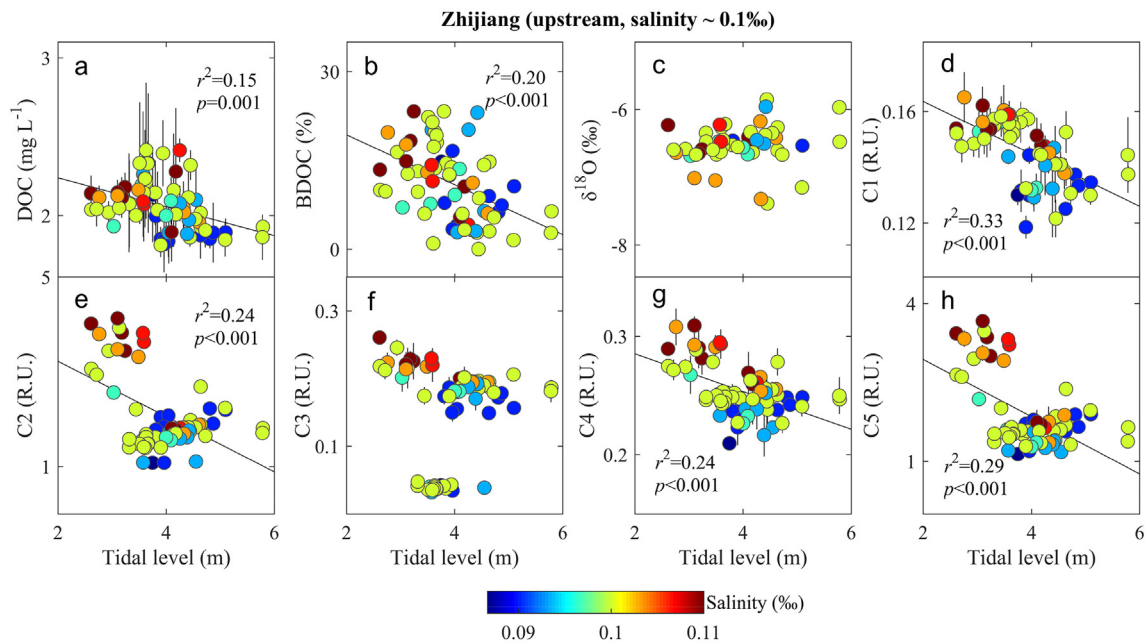


Fig. 3. Relationships between tidal level and mean dissolved organic carbon (DOC) (a), mean bioavailable DOC (BDOC) (b), stable isotopic $\delta^{18}\text{O}$ (c), mean F_{max} of terrestrial humic-like C1 (d), tryptophan-like C2 (e), agricultural humic-like C3 (f), microbial humic-like C4 (g), and blue-shifted tryptophan-like C5 (h) for the samples collected from Zhijiang (salinity ~0.1‰) in the upstream of the Qiantang estuary. Error bars represent ± 1 S.D. of triplicate samples. Color in all panels stand for the corresponding salinity.

relationships were observed between salinity and DOC, BDOC, terrestrial humic-like C1, and microbial humic-like C4 ($p < 0.01$, Fig. S13), while significant positive relationships were recorded between salinity and $\delta^{18}\text{O}$ and between salinity and agricultural humic-like C3 ($p < 0.01$, Fig. S13). No significant relationship was recorded between salinity with either C2 or C5–C6 (Fig. S13).

3.5. PCA modeling results

For the samples collected from the Zhijiang upstream site, the first two principal components, PC1 and PC2, accounted for 40.5% and 30.6%, respectively, of the variability in DOM-related parameters

included in the PCA (Fig. 5). BDOC, and PARAFAC components C1–C5 exhibited positive PC1 loadings, while SPM, DOC, $\delta^{13}\text{C}$ -DOC, and tyrosine-like C6 demonstrated negative PC1 loadings (Fig. 5). As Zhijiang is surrounded by the highly urbanized metropolitan city of Hangzhou, and tryptophan-like C2 and C5 and microbial humic-like C4 displayed high PC1 loadings (Fig. 5), Chl-*a* in the Qiantang estuary is often very low ($< 5 \mu\text{g L}^{-1}$, (Wang et al., 2007)) and PC1 was therefore closely linked with the anthropogenic tryptophan-like input. DOC, BDOC and terrestrial humic-like C1 showed high PC2 loading (Fig. 6), indicating that PC2 may be positively related to the terrestrial CDOM input. Tidal level correlated negatively with PC1 and PC2 ($p < 0.001$, Fig. 6). In comparison, positive relationships were observed between

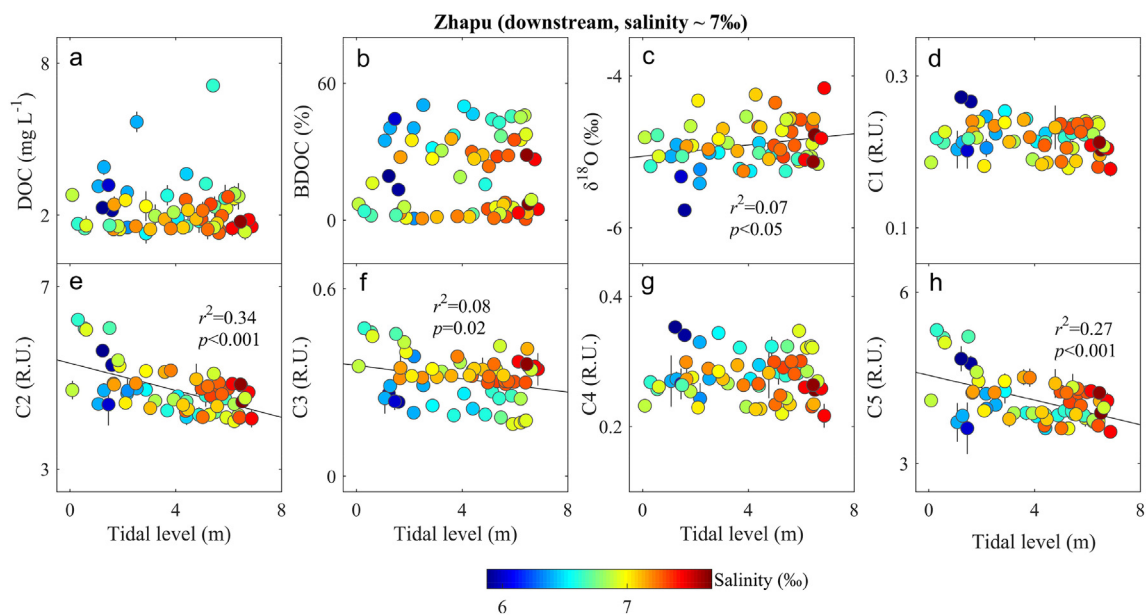


Fig. 4. Relationships between tidal level and dissolved organic carbon (DOC) (a), bioavailable DOC (BDOC) (b), stable isotopic $\delta^{18}\text{O}$ (c), and the PARAFAC-derived components C1–C5 (d–h) for the samples collected from Zhapu (salinity ~7‰) in the downstream of the Qiantang estuary. Error bars represent ± 1 S.D. of triplicate samples. Color in all panels stand for the corresponding salinity.

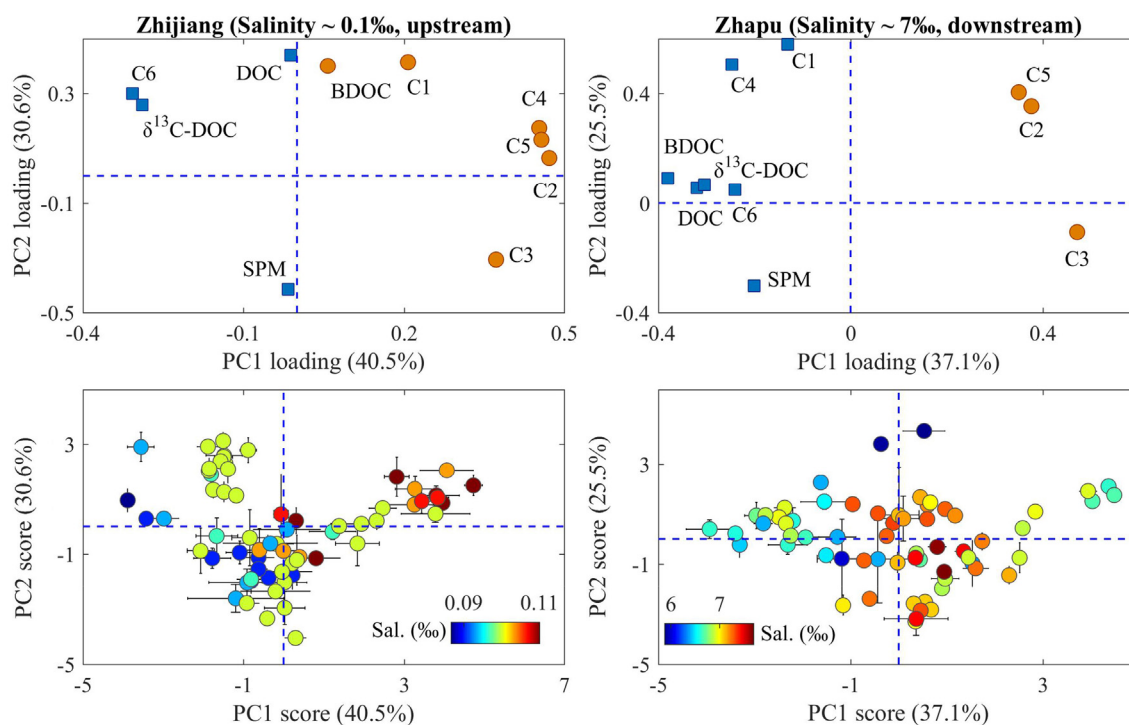


Fig. 5. PCA factor loadings and scores for samples collected from upstream Zhijiang (a–b) and downstream Zhapu (c–d). Error bars in the lower panels represent ± 1 S.D. of triplicate samples; color in panel b and d denote the salinity at Zhijiang and Zhapu, respectively.

salinity and PC1 ($p < 0.01$), PC2 ($p < 0.05$) at the Zhijiang upstream site (Fig. 6).

In comparison, at the downstream Zhapu, PC1 and PC2 explained 37.1% and 25.5%, respectively, of total variability (Fig. 5). Tryptophan-like C2 and C5 and agricultural humic-like C3 displayed high PC1 loadings, while SPM, DOC, BDOC, $\delta^{13}\text{C}$ -DOC, terrestrial humic-like C1, microbial humic-like C4, and tyrosine-like C6 exhibited negative PC1 loadings (Fig. 5). Zhapu is surrounded by highly urbanized residential areas and this suggests that PC1 at Zhapu is also positively related to the anthropogenic tryptophan-like input. Tryptophan-like C2 and C5 coupled with terrestrial humic-like C1 all exhibited high PC2 loadings (Fig. 5),

implying that PC2 is also positively linked with the anthropogenic input. The tidal level correlated negatively with PC1 and PC2 ($p < 0.01$, Fig. 6), and salinity correlated negatively with PC2 ($p < 0.01$, Fig. 6), while a weak but positive relationship was observed between salinity and PC1 ($p < 0.05$, Fig. 6).

3.6. FT-ICR MS results

Solid-phase extracted samples collected from Zhijiang and Zhapu contained 11,333 and 12,702 assigned formula peaks (Fig. 7). Terrestrial lignin molecules displayed 8163 and 8999 peaks, corresponding to

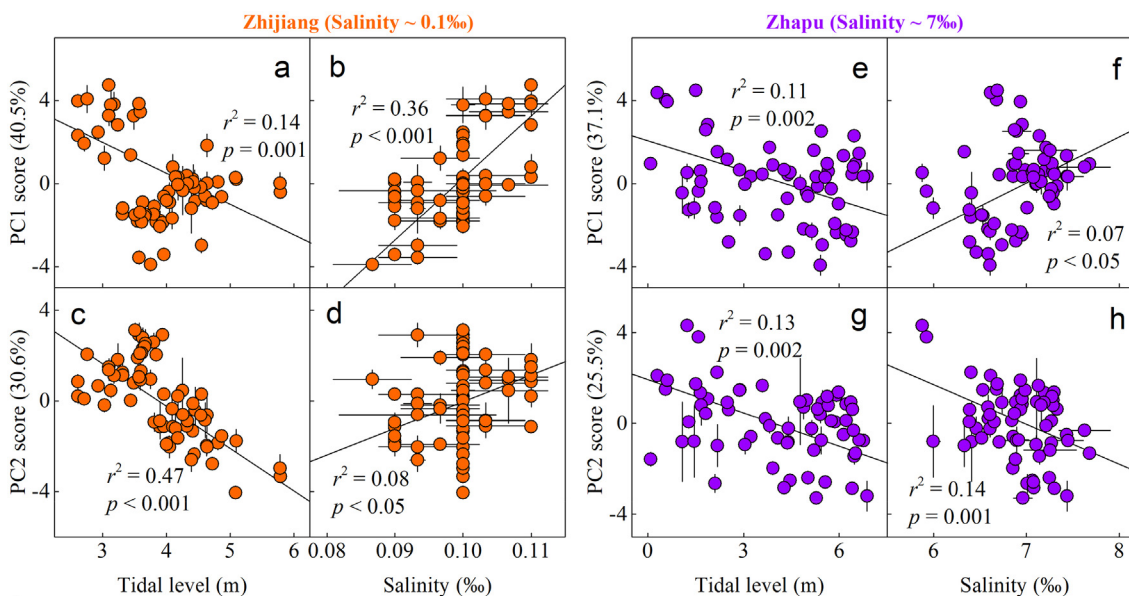


Fig. 6. Relationships between PC1 score and tidal level (a), salinity (b), and between PC2 and tidal level (c), salinity (d) at Zhijiang (salinity ~0.1‰, upstream) and Zhapu (salinity ~7‰, downstream, e–h). PC1 and PC2 scores can be found in Fig. 5. Error bars in all panels represent ± 1 S.D. of triplicate samples.

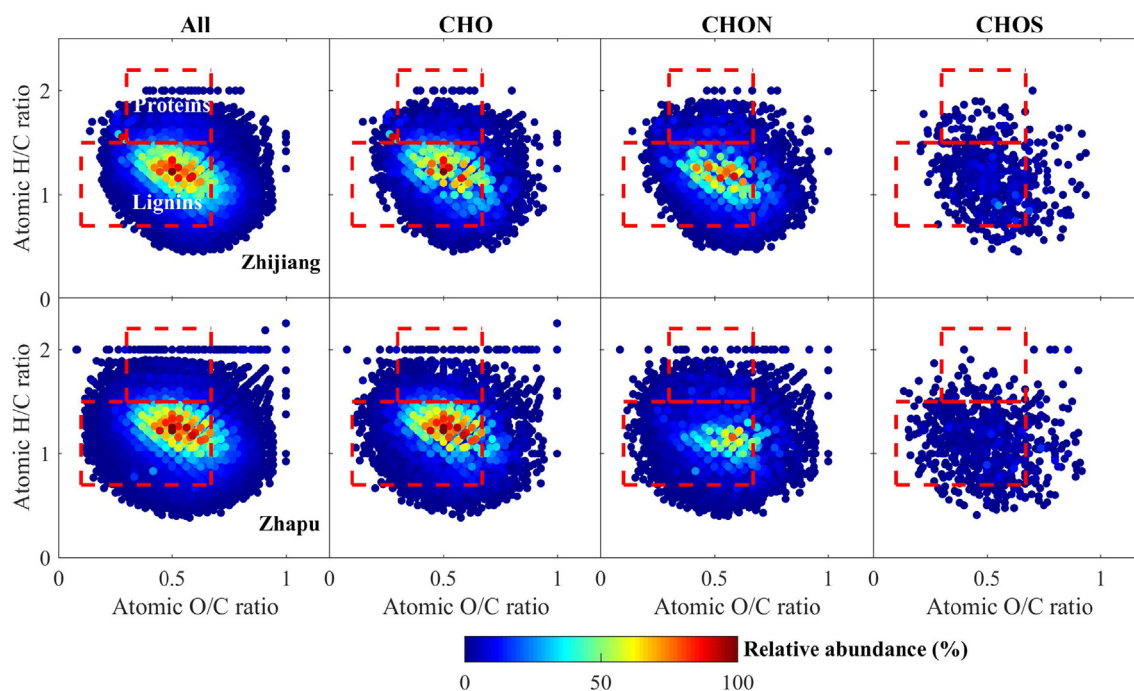


Fig. 7. van Krevelen diagrams of the distribution of bulk DOM samples collected from Zhijiang (upper panels) and Zhapu (lower panels). Colors in the two panels represent the relative abundance of the FT-ICR MS signals. The 1st to 4th column panels are the van Krevelen diagrams of the distributions of all, carbohydrates (CHO), nitrogen-containing compounds (CHON), and sulphur-containing compounds (CHOS), respectively. The dash lines circled areas are assigned protein and lignin molecules, respectively in all panels.

contribution percentages of 72% and 71% of the number of total assigned formulas for the samples collected from Zhijiang and Zhapu, respectively (Fig. 7; Table S2). In comparison, protein displayed 1248 and 1222 peaks and corresponded to 11% and 10%, respectively, of the samples collected from Zhijiang and Zhapu (Fig. 7; Table S2). The formulas associated with terrestrial lignin molecules exhibited high relative abundance compared with formulas associated with other compound classes (Fig. 7). Both Zhijiang and Zhapu contained high proportions of carbohydrates (CHO) (42% for both Zhijiang and Zhapu) and nitrogen-containing compounds (CHON) formulas (47% and 46% for Zhijiang and Zhapu, respectively; Fig. 7). It is noted that the CHON compounds were more closely linked to terrestrial lignins at Zhapu than at Zhijiang (Fig. 7).

4. Discussion

Our results suggest that tidal fluctuations by largely controlling the physical mixing of freshwater and saltwater, and also surface and deep layers in the water column, to a large extent affect the optical dynamics and bioavailability of terrestrial and anthropogenic CDOM in the Qiantang estuary with surrounding areas highly urbanized.

Firstly, DOC, $a(254)$, in situ measured FDOM, and F_{\max} values of C1–C5 all decreased with increasing salinity during the extensive field sampling campaign (Fig. 2), which suggests that the Qiantang River carried a mixture of terrestrial humic-rich and anthropogenic protein-rich CDOM and contributed primarily to the CDOM pool in the estuary. The mean F_{\max} values of tryptophan-like C2 and C5 were notably higher than those of the other four components and are derived from either degradation products of algal block mass (Yamashita and Tanoue, 2004; Stedmon and Markager, 2005b; Zhang et al., 2009; Zhou et al., 2015) or household sewage (Stedmon et al., 2011; Zhou et al., 2016a). However, mean Chl-*a* in the Qiantang estuary typically ranges from ~2 to ~4 $\mu\text{g L}^{-1}$ (Wang et al., 2007), and the degradation of algae cells therefore most likely contributes little to the CDOM pool in the estuary compared with anthropogenic CDOM. The high F_{\max} of tryptophan-like fluorophores in the estuary and at both Zhijiang and Zhapu might,

therefore, be explained by discharges of household sewage from the surrounding highly urbanized areas (Fig. 1).

Secondly, continuous observations made upstream of the Qiantang estuary at Zhijiang (salinity ~0.1‰) showed that DOC, BDOC, terrestrial humic-like C1, tryptophan-like C2 and C5, and microbial humic-like C4 decreased with increasing tidal level (Fig. 3) provided further evidence. This suggests that ebb tides with terrestrial soil organic matter from upstream Qiantang River and residential sewage from the surrounding metropolitan Hangzhou City will result in higher concentrations of DOC with higher bioavailability than flood tides. The tidal level at Zhijiang is controlled by a combined effect of the Qiantang river flow and the backwater of the estuary tides (Fig. S14), and ebb tides are usually coupled with low upstream inflow discharge, prolonged water residence time, and increased salinity (Fig. S14). The positive relationships between salinity and DOC and between salinity and the F_{\max} values of C1–C5 at the upstream of Zhijiang (salinity ~0.1‰, Fig. S14) provide further evidence of this. Point-source contaminated waters from the surrounding highly urbanized residential areas during ebb tides carry high concentrations of DOC that are discharged to the estuary, and this portion of DOC is usually highly bioavailable (Baker, 2001; Zhou et al., 2016a).

Thirdly, the negative relationships between tidal level and tryptophan-like C2 and C5, and agricultural humic-like C3 (Fig. 4) at Zhapu (salinity ~7‰, downstream) provide further evidence of a higher influence of ebb tides. Thus, ebb tides enhanced the discharge of household sewage from the surrounding Zhapu town to the receiving waters. The negative relationships between salinity and DOC, BDOC, and the F_{\max} values of terrestrial humic-like C1 and agricultural humic-like C4 (Fig. S13) therefore implying that ebb tides enhance terrestrial and anthropogenic CDOM. This is further evidenced by the positive relationship between tidal level and $\delta^{18}\text{O}$ (Fig. 4) as riverine freshwater usually has more depleted $\delta^{18}\text{O}$ than saltwater (Stedmon et al., 2015), and saltwater carried by flood tide therefore displayed enriched $\delta^{18}\text{O}$ (Fig. S13). This was substantiated by the positive relationship between salinity and $\delta^{18}\text{O}$ at Zhapu (Fig. S13). Zhapu is located at the north shore of the estuary, and tidal oscillations here can not only fuel the mixing of freshwater and saltwater but also the mixing of the surface

and bottom layers of the water column (He et al., 2013), which is supported by the high SPM during the flood tide here (Fig. S1). This and the limited sampling periods and sites might explain the lack of a significant relationship between tidal level and DOC or BDOC, or between salinity and tryptophan-like C2 or C5 (Fig. 4; Fig. S13). Future works can benefit from seasonal sampling collection to be able to including more end member samples, and also the application of online real-time fluorescence sensor and high temporal resolution remote sensing images (He et al., 2013).

Fourthly, the tidal oscillation impact on the highly urbanized Qiantang estuary is supported by the PCA results for both upstream Zhijiang and downstream Zhapu (Fig. 5; Fig. 6). PC1 at the upstream Zhijiang is positively linked with the anthropogenic CDOM input and increased with increasing salinity and with decreasing tidal level (Fig. 6), which suggested that with diminished freshwater discharge and longer water residence time, the concentration of anthropogenic CDOM here may rise. In contrast, an increased flow rate of the Qiantang river through the backwater can result in increased tidal level (He et al., 2013) and subsequently diluted anthropogenic tryptophan-like signals. This is substantiated by the fact that Lake Qiandao in the upstream Xin'anjiang river system is a national key drinking water source with a consequently low discharge of DOC concentrations downstream (Zhou et al., 2016b). Also the negative relationships between tidal level and PC1–PC2 scores at the downstream Zhapu (Fig. 6), all being positively related to anthropogenic tryptophan-like substances (Fig. 5), point in direction of tidal oscillation impact, this is further substantiated by the negative relationship between salinity and PC2 scores (Fig. 6). Seawater with a relatively high salinity carried by flood tides flushed freshwater backwards, consequently diluting the anthropogenic tryptophan-like signals here at the downstream Zhapu (Fig. 6).

The switch from flood tides to ebb tides shifts the CDOM sources from turbid seawater with low DOC to clean riverine freshwater with high anthropogenic tryptophan-rich DOM and BDOC, especially in the downstream of the estuary (Figs. 3–6), as revealed by the positive relationship between tidal level and salinity discovered here (Fig. S14). Anthropogenic CDOM derived from upstream and surrounding residential areas was closely coupled with terrestrial humic-rich substances, as shown by the relationships between salinity and these fluorescence signals (Figs. 2–4), and the close linkages between nitrogen-containing compounds and terrestrial lignins revealed by FT-ICR MS, especially for the downstream Zhapu site (Fig. 7). The similar FT-ICR MS results between Zhijiang and Zhapu can be explained by both sites receiving terrestrial and anthropogenic CDOM input simultaneously as supported by similar fluorescent spectra between these two sites (Fig. 3; Fig. 4; Table 1). Note that the numbers of peak identified for different compound classes can also be influenced by the ionization efficiency (Stubbins et al., 2010; Spencer et al., 2014). Massive discharge to the estuary from the Qiantang River, the largest river in the Zhejiang Province in China, is usually encounter with the backwater carried by flood tides, and this controls the tidal levels at the upstream Zhijiang (Fig. S14). This explained the negative relationships between tidal level and salinity at Zhijiang (Fig. S14). The gravity in the Earth's rotation fuels the formation of main deep channel in the southern half of the estuary and the northern half tidal-flat area, and compared with the northern half, the southern half channel receives little sewage from the north intense residential areas and therefore better representing freshwater and marine water mixing (Fig. 2).

In sum, our results collectively suggest that the concentration, optical dynamics, and bioavailability (and thus likely the metabolism) of CDOM in the Qiantang estuary were impacted by a combination of anthropogenic sewage discharge and terrestrial soil organic matter input and tidal oscillations. The semi-diurnal alternations between the elevated DOC and BDOC induced by ebbs with enhanced riverine anthropogenic input and reduced DOC and BDOC caused by flood tides with enhanced seawater dilution effects support the ecosystem sustainability of the Qiantang estuary.

Acknowledgments

This study was jointly funded by the Strategic Priority Research Program of the Chinese Academy of Sciences (XDA19080304), the National Natural Science Foundation of China (grants 41807362, 41621002, and 41501374), the Natural Science Foundation of Jiangsu Province (BK20181104) and Natural Science Foundation of Zhejiang Province (LQ16D010001) and NIGLAS Foundation (NIGLAS2017QD08) in China. Erik Jeppesen was supported by the AU Centre for Water Technology (WATEC.AU.DK). The work partially supported by NSF (DMR-1157490), State of Florida, and the FSU Future Fuels Institute. The authors thank Donald F. Smith and all the other people in the NHMFL ICR Program that work selflessly to facilitate data acquisition and processing for users of the facility. We would like to express our deep thanks to Anne Mette Poulsen from Aarhus University for editorial assistance. We would also like to thank Jian Huang, Zhong Xia, Ningchao Liu, Shiwen Huang, and Chengying Zhang for their help with field sample collection and laboratory measurements. The data used in the paper are available upon request to Dr. Yunlin Zhang (ylzhang@niglas.ac.cn). The authors are grateful to the editor Prof. Yolanda Pico and the five anonymous reviewers for their helpful comments and suggestions.

Appendix A. Supplementary data

Supplementary data to this article can be found online at <https://doi.org/10.1016/j.scitotenv.2019.01.220>.

References

- Abbott, B.W., Larouche, J.R., Jones, J.B., Bowden, W.B., Balsler, A.W., 2014. Elevated dissolved organic carbon biodegradability from thawing and collapsing permafrost. *J. Geophys. Res. Biogeosci.* 119, 2049–2063.
- Baker, A., 2001. Fluorescence excitation-emission matrix characterization of some sewage-impacted rivers. *Environ. Sci. Technol.* 35, 948–953.
- Bianchi, T.S., Garcia-Tigeros, F., Yvon-Lewis, S.A., Shields, M., Mills, H.J., Butman, D., et al., 2013. Enhanced transfer of terrestrially derived carbon to the atmosphere in a flooding event. *Geophys. Res. Lett.* 40, 116–122. <https://doi.org/10.1029/2012gl054145>.
- Bro, R., Smilde, A.K., 2014. Principal component analysis. *Anal. Methods* 6, 2812–2831. <https://doi.org/10.1039/c3ay41907j>.
- Carey, J.C., Fulweiler, R.W., 2014. Salt marsh tidal exchange increases residence time of silica in estuaries. *Limnol. Oceanogr.* 59, 1203–1212. <https://doi.org/10.4319/lo.2014.59.4.1203>.
- Corilo Y. EnviroOrg. 2015: Florida State University. doi:10.5846/.
- Guo, W., Yang, L., Zhai, W., Chen, W., Osburn, C.L., Huang, X., et al., 2014. Runoff-mediated seasonal oscillation in the dynamics of dissolved organic matter in different branches of a large bifurcated estuary—the Changjiang estuary. *J. Geophys. Res. Biogeosci.* 119, 776–793. <https://doi.org/10.1002/2013jg002540>.
- He, X., Bai, Y., Pan, D., Huang, N., Dong, X., Chen, J., et al., 2013. Using geostationary satellite ocean color data to map the diurnal dynamics of suspended particulate matter in coastal waters. *Remote Sens. Environ.* 133, 225–239. <https://doi.org/10.1016/j.rse.2013.01.023>.
- Holmes, R.M., McClelland, J.W., Raymond, P.A., Frazer, B.B., Peterson, B.J., Stieglitz, M., 2008. Lability of DOC transported by Alaskan rivers to the Arctic Ocean. *Geophys. Res. Lett.* 35, L03402. <https://doi.org/10.1029/2007gl032837>.
- Hood, E., Fellman, J., Spencer, R.G., Hernes, P.J., Edwards, R., D'Amore, D., et al., 2009. Glaciers as a source of ancient and labile organic matter to the marine environment. *Nature* 462, 1044–1047. <https://doi.org/10.1038/nature08580>.
- Huang, C., Jiang, Q., Yao, L., Yang, H., Lin, C., Huang, T., et al., 2018. Variation pattern of particulate organic carbon and nitrogen in oceans and inland waters. *Biogeosciences* 15, 1827–1841.
- Hur, J., Jung, K.Y., Schlautman, M.A., 2011. Altering the characteristics of a leaf litter-derived humic substance by adsorptive fractionation versus simulated solar irradiation. *Water Res.* 45, 6217–6226. <https://doi.org/10.1016/j.watres.2011.09.023>.
- Kothawala, D.N., Stedmon, C.A., Muller, R.A., Weyhenmeyer, G.A., Kohler, S.J., Tranvik, L.J., 2014. Controls of dissolved organic matter quality: evidence from a large-scale boreal lake survey. *Glob. Chang. Biol.* 20, 1101–1114. <https://doi.org/10.1111/gcb.12488>.
- Kowalczyk, P., Durako, M.J., Young, H., Kahn, A.E., Cooper, W.J., Gonsior, M., 2009. Characterization of dissolved organic matter fluorescence in the South Atlantic bight with use of PARAFAC model: interannual variability. *Mar. Chem.* 113, 182–196. <https://doi.org/10.1016/j.marchem.2009.01.015>.
- Kowalczyk, P., Tilstone, G.H., Zablocka, M., Röttgers, R., Thomas, R., 2013. Composition of dissolved organic matter along an Atlantic meridional transect from fluorescence spectroscopy and parallel factor analysis. *Mar. Chem.* 157, 170–184. <https://doi.org/10.1016/j.marchem.2013.10.004>.
- Maie, N., Scully, N.M., Pisani, O., Jaffé, R., 2007. Composition of a protein-like fluorophore of dissolved organic matter in coastal wetland and estuarine ecosystems. *Water Res.* 41, 563–570.

- Mei, W., Xie, S.-P., 2016. Intensification of landfalling typhoons over the Northwest Pacific since the late 1970s. *Nat. Geosci.* 9, 753–757. <https://doi.org/10.1038/ngeo2792>.
- Murphy, K.R., Stedmon, C.A., Waite, T.D., Ruiz, G.M., 2008. Distinguishing between terrestrial and autochthonous organic matter sources in marine environments using fluorescence spectroscopy. *Mar. Chem.* 108, 40–58. <https://doi.org/10.1016/j.marchem.2007.10.003>.
- Murphy, K.R., Hambly, A., Singh, S., Henderson, R.K., Baker, A., Stuetz, R., et al., 2011. Organic matter fluorescence in municipal water recycling schemes: toward a unified PARAFAC model. *Environ. Sci. Technol.* 45, 2909–2916. <https://doi.org/10.1021/es103015e>.
- Murphy, K.R., Stedmon, C.A., Graeber, D., Bro, R., 2013. Fluorescence spectroscopy and multi-way techniques. *PARAFAC. Anal. Methods* 5, 6557–6566. <https://doi.org/10.1039/c3ay41160e>.
- Murphy, K.R., Stedmon, C.A., Wenig, P., Bro, R., 2014. OpenFluor—an online spectral library of auto-fluorescence by organic compounds in the environment. *Anal. Methods* 6, 658–661. <https://doi.org/10.1039/c3ay41935e>.
- Nicholls, R., Hutton, C., Lázár, A., Allan, A., Adger, W., Adams, H., et al., 2016. Integrated assessment of social and environmental sustainability dynamics in the Ganges-Brahmaputra-Meghna delta, Bangladesh. *Estuar. Coast. Shelf Sci.* 183, 370–381.
- Ohno, T., Parr, T.B., Gruselle, M.C., Fernandez, I.J., Sleighter, R.L., Hatcher, P.G., 2014. Molecular composition and biodegradability of soil organic matter: a case study comparing two new England forest types. *Environ. Sci. Technol.* 48, 7229–7236. <https://doi.org/10.1021/es405570c>.
- Osburn, C.L., Wigdahl, C.R., Fritz, S.C., Saros, J.E., 2011. Dissolved organic matter composition and photoreactivity in prairie lakes of the U.S. Great Plains. *Limnol. Oceanogr.* 56, 2371–2390. <https://doi.org/10.4319/lo.2011.56.6.2371>.
- Osburn, C.L., Handsel, L.T., Mikan, M.P., Paerl, H.W., Montgomery, M.T., 2012. Fluorescence tracking of dissolved and particulate organic matter quality in a river-dominated estuary. *Environ. Sci. Technol.* 46, 8628–8636. <https://doi.org/10.1021/es3007723>.
- Paerl, H.W., Huisman, J., 2008. Climate. Blooms like it hot. *Science* 320, 57–58.
- Paerl, H.W., Hall, N.S., Peierls, B.L., Rossignol, K.L., Joyner, A.R., 2013. Hydrologic variability and its control of phytoplankton community structure and function in two shallow, coastal, lagoonal ecosystems: the Neuse and New River estuaries, North Carolina, USA. *Estuar. Coasts* 37, 31–45. <https://doi.org/10.1007/s12237-013-9686-0>.
- Shen, C., Zhang, C., Jin, G., Kong, J., Li, L., 2016. Effects of unstable flow on solute transport in the marsh soil and exchange with coastal water. *Geophys. Res. Lett.* 43, 12,091–12,101. <https://doi.org/10.1002/2016gl070576>.
- Shutova, Y., Baker, A., Bridgeman, J., Henderson, R.K., 2014. Spectroscopic characterisation of dissolved organic matter changes in drinking water treatment: from PARAFAC analysis to online monitoring wavelengths. *Water Res.* 54, 159–169. <https://doi.org/10.1016/j.watres.2014.01.053>.
- Smith, D.F., Podgorski, D.C., Rodgers, R.P., Blakney, G.T., Hendrickson, C.L., 2018. 21 tesla FT-ICR mass spectrometer for ultrahigh-resolution analysis of complex organic mixtures. *Anal. Chem.* 90, 2041–2047. <https://doi.org/10.1021/acs.analchem.7b04159>.
- Spencer, R.G.M., Guo, W., Raymond, P.A., Dittmar, T., Hood, E., Fellman, J., et al., 2014. Source and biolability of ancient dissolved organic matter in glacier and lake ecosystems on the Tibetan plateau. *Geochim. Cosmochim. Acta* 142, 64–74. <https://doi.org/10.1016/j.gca.2014.08.006>.
- Stedmon, C.A., Bro, R., 2008. Characterizing dissolved organic matter fluorescence with parallel factor analysis: a tutorial. *Limnol. Oceanogr. Methods* 6, 572–579. <https://doi.org/10.4319/lom.2008.6.572b>.
- Stedmon, C.A., Markager, S., 2005a. Resolving the variability in dissolved organic matter fluorescence in a temperate estuary and its catchment using PARAFAC analysis. *Limnol. Oceanogr.* 50, 686–697. <https://doi.org/10.4319/lo.2005.50.2.0686>.
- Stedmon, C.A., Markager, S., 2005b. Tracing the production and degradation of autochthonous fractions of dissolved organic matter by fluorescence analysis. *Limnol. Oceanogr.* 50, 1415–1426. <https://doi.org/10.4319/lo.2005.50.5.1415>.
- Stedmon, C.A., Sereyńska-Sobecka, B., Boe-Hansen, R., Le Tallec, N., Waul, C.K., Arvin, E., 2011. A potential approach for monitoring drinking water quality from groundwater systems using organic matter fluorescence as an early warning for contamination events. *Water Res.* 45, 6030–6038. <https://doi.org/10.1016/j.watres.2011.08.066>.
- Stedmon, C.A., Granskog, M., Dodd, P.A., 2015. An approach to estimate the freshwater contribution from glacial melt and precipitation in East Greenland shelf waters using colored dissolved organic matter (CDOM). *J. Geophys. Res. Oceans* 120, 1107–1117. <https://doi.org/10.1002/2014JC010501>.
- Stubbins, A., Spencer, R.G.M., Chen, H., Hatcher, P.G., Mopper, K., Hernes, P.J., et al., 2010. Illuminated darkness: molecular signatures of Congo River dissolved organic matter and its photochemical alteration as revealed by ultrahigh precision mass spectrometry. *Limnol. Oceanogr.* 55, 1467–1477. <https://doi.org/10.4319/lo.2010.55.4.1467>.
- Vonk, J.E., Tank, S.E., Mann, P.J., Spencer, R.G.M., Treat, C.C., Striegl, R.G., et al., 2015. Biodegradability of dissolved organic carbon in permafrost soils and aquatic systems: a meta-analysis. *Biogeosciences* 12, 6915–6930. <https://doi.org/10.5194/bg-12-6915-2015>.
- Wang, M., Tang, J., Shi, W., 2007. MODIS-derived ocean color products along the China east coastal region. *Geophys. Res. Lett.* 34, L06611. <https://doi.org/10.1029/2006gl028599>.
- Ward, N.D., Krusche, A.V., Sawakuchi, H.O., Brito, D.C., Cunha, A.C., Moura, J.M.S., et al., 2015. The compositional evolution of dissolved and particulate organic matter along the lower Amazon River—Óbidos to the ocean. *Mar. Chem.* 177, 244–256. <https://doi.org/10.1016/j.marchem.2015.06.013>.
- Wu, H., Li, X., Li, J., Jiang, Z., Li, G., Liu, L., 2015. Evaporative enrichment of stable isotopes ($\delta^{18}\text{O}$ and δD) in lake water and the relation to lake-level change of Lake Qinghai, northeast Tibetan plateau of China. *J. Arid. Land* 7, 623–635. <https://doi.org/10.1007/s40333-015-0048-6>.
- Xie, D., Pan, C., Wu, X., Gao, S., Wang, Z., 2017. The variations of sediment transport patterns in the outer Changjiang estuary and Hangzhou Bay over the last 30 years. *J. Geophys. Res. Oceans* 122, 2999–3020.
- Yamamoto-Kawai, M., McLaughlin, F.A., Carmack, E.C., Nishino, S., Shimada, K., 2008. Freshwater budget of the Canada Basin, Arctic Ocean, from salinity, $\delta^{18}\text{O}$, and nutrients. *J. Geophys. Res.* 113, C01007. <https://doi.org/10.1029/2006jc003858>.
- Yamashita, Y., Tanoue, E., 2004. In situ production of chromophoric dissolved organic matter in coastal environments. *Geophys. Res. Lett.* 31, L14302. <https://doi.org/10.1029/2004gl019734>.
- Yamashita, Y., Jaffé, R., Maie, N., Tanoue, E., 2008. Assessing the dynamics of dissolved organic matter (DOM) in coastal environments by excitation emission matrix fluorescence and parallel factor analysis (EEM-PARAFAC). *Limnol. Oceanogr.* 53, 1900–1908. <https://doi.org/10.4319/lo.2008.53.5.1900>.
- Yang, L., Yang, W., Hong, H., Wang, G., 2013. Non-conservative behaviors of chromophoric dissolved organic matter in a turbid estuary: roles of multiple biogeochemical processes. *Estuar. Coast. Shelf Sci.* 133, 285–292. <https://doi.org/10.1016/j.ecss.2013.09.007>.
- Yang, L., Zhuang, W.E., Chen, C.A., Wang, B.J., Kuo, F.W., 2017. Unveiling the transformation and bioavailability of dissolved organic matter in contrasting hydrothermal vents using fluorescence EEM-PARAFAC. *Water Res.* 111, 195–203. <https://doi.org/10.1016/j.watres.2017.01.001>.
- Zhang, Y., van Dijk, M.A., Liu, M., Zhu, G., Qin, B., 2009. The contribution of phytoplankton degradation to chromophoric dissolved organic matter (CDOM) in eutrophic shallow lakes: field and experimental evidence. *Water Res.* 43, 4685–4697. <https://doi.org/10.1016/j.watres.2009.07.024>.
- Zhou, Y., Jeppesen, E., Zhang, Y., Niu, C., Shi, K., Liu, X., et al., 2015. Chromophoric dissolved organic matter of black waters in a highly eutrophic Chinese lake: freshly produced from algal scums? *J. Hazard. Mater.* 299, 222–230. <https://doi.org/10.1016/j.jhazmat.2015.06.024>.
- Zhou, Y., Jeppesen, E., Zhang, Y., Shi, K., Liu, X., Zhu, G., 2016a. Dissolved organic matter fluorescence at wavelength 275/342 nm as a key indicator for detection of point-source contamination in a large Chinese drinking water lake. *Chemosphere* 144, 503–509. <https://doi.org/10.1016/j.chemosphere.2015.09.027>.
- Zhou, Y., Zhang, Y., Jeppesen, E., Murphy, K.R., Shi, K., Liu, M., et al., 2016b. Inflow rate-driven changes in the composition and dynamics of chromophoric dissolved organic matter in a large drinking water lake. *Water Res.* 100, 211–221. <https://doi.org/10.1016/j.watres.2016.05.021>.
- Zhou, Y., Zhou, J., Jeppesen, E., Zhang, Y., Qin, B., Shi, K., et al., 2016c. Will enhanced turbulence in inland waters result in elevated production of autochthonous dissolved organic matter? *Sci. Total Environ.* 543, 405–415. <https://doi.org/10.1016/j.scitotenv.2015.11.051>.
- Zhou, Y., Shi, K., Zhang, Y., Jeppesen, E., Liu, X., Zhou, Q., et al., 2017. Fluorescence peak integration ratio IC:IT as a new potential indicator tracing the compositional changes in chromophoric dissolved organic matter. *Sci. Total Environ.* 574, 1588–1598. <https://doi.org/10.1016/j.scitotenv.2016.08.196>.